Nonlinearity Analysis of Analog/RF Circuits Using Combined Multisine and Volterra Analysis

Jonathan Borremans[1,2], Ludwig De Locht[1,2], Piet Wambacq[1,2] and Yves Rolain[2]
[1]IMEC, Leuven, Belgium - [2]Vrije Universiteit Brussel, Brussels, Belgium

***Abstract*— Modern integrated radio systems require highly linear analog/RF circuits. Two-tone simulations are commonly used to study a circuit's nonlinear behavior. Very often, however, this approach suffers limited insight. To gain insight into nonlinear behavior, we use a multisine analysis methodology to locate the main nonlinear components (e.g. transistors) both for weakly and strongly nonlinear behavior. Under weakly nonlinear conditions, selective Volterra analysis is used to further determine the most important nonlinearities of the main nonlinear components. As shown with an example of a 90 nm CMOS wideband low-noise amplifier, the insights obtained with this approach can be used to reduce nonlinear circuit behavior, in this case with 10 dB. The approach is valid for wideband and thus practical excitation signals, and is easily applicable both to simple and complex circuits.**

I. Introduction

Nonlinear behavior in radio circuits causes problems such as distortion, crosstalk and desensitization. Numerical circuit simulations provide acceptable results, but they give no indication on which nonlinearities are mainly responsible for the observed behavior. Different numerical approaches to gain insight in nonlinear circuit behavior have been published. They decompose the circuit's overall nonlinear behavior into different contributions. Approaches [8], [5] are based on Volterra series for time-invariant or periodically time-varying weakly nonlinear circuits. For a given order n (typically limited to three), they decompose the nonlinear behavior into contributions. These correspond to every coefficient from order 2 to n in the power series that describes a nonlinearity. Although this approach yields insight, it is complex due to the large number of contributions. For example, the drain current of one MOS transistor with body effect gives rise to sixteen contributions. Clearly, if one also takes into account the nonlinear capacitors, circuits of practical size suffer from enormous complexity.

At the expense of reduced insight, the per-nonlinearity distortion analysis of [6], which is limited to weakly nonlinear behavior, splits the nonlinear behavior of a circuit into less contributions. For example, for a MOS transistor, the drain current is treated here as one single contribution. This allows to identify the transistors that contribute most to the nonlinear behavior. However, no information is given about which nonlinearity of the drain current (e.g. the nonlinear dependence on v_{GS} or on v_{DS}) is responsible for the observed nonlinear behavior.

The multisine approach used in our work also splits the nonlinear behavior in similar contributions as in [6], but it is able to deal with strongly nonlinear behavior, e.g. caused by clipping. In this way, it yields similar information as the per-nonlinearity distortion analysis mentioned above, but now extended to strongly nonlinear behavior. Further, if a circuit behaves in a weakly nonlinear way, additional insight can be gained by using a selective Volterra analysis based on the results of the multisine analysis. The Volterra analysis now only takes into account the nonlinearity of the transistors identified with the multisine analysis as main contributors to the observed nonlinear behavior. In this way, the cumbersome and time consuming bookkeeping of Volterra analysis is circumvented as the number of contributions is highly reduced. The extra insight offered with Volterra analysis gives an even better indication than the multisine analysis or the per-nonlinearity analysis on how to improve a circuit's nonlinear behavior.

The proposed combination of multisine analysis and selective Volterra analysis is illustrated here with the design of a wideband low-noise amplifier (LNA), where the IIP_3 of a standard design has been increased by 10 dB thanks to a change of the bias point of the most contributing transistor.

Section II introduces the use of multisines for the study of nonlinear behavior. Section III introduces the concept of applying selective Volterra analysis and Section IV illustrates the proposed methodology on the LNA.

II. Multisine methodology

A. Multisines

A multisine is a periodic signal consisting of a sum of N sinusoidal signals that are commensurate in frequency [2]:

$$s(t) = \frac{1}{\sqrt{N}} \sum_{k=1}^{N} \hat{R}_k cos(2\pi f_k t + \varphi_k) \tag{1}$$

in which $\hat{R}_k$ and φ_k are the amplitude and random phases, respectively. Further, $f_k = k.f_{max}/N$ is the frequency of the k^{th} sinusoid. Multisines can be chosen in a particular way to distinguish even-order and odd-order nonlinear behavior. A selection of $f_k = f_1.k$ tones with k odd is selected for the multisine with f_1 being the fundamental frequency. This means that R_k is equal to zero for k even in Eq. 1. As a result the level of even-order distortion is found at the even frequency components of the output spectrum. Indeed, odd (excited) frequency components result in even (non-excited) frequency components by an even-order nonlinear system.

978-3-9810801-2-4/DATE07 © 2007 EDAA

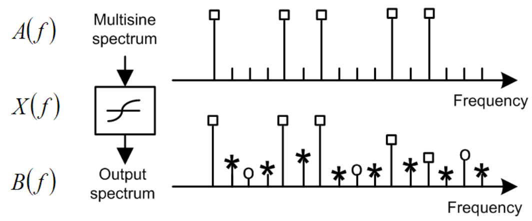

Fig. 1. Concept of a multisine excitation signal to distinguish odd-order and even-order nonlinear behavior. Odd-order generated distortion is marked with 'o', even-order distortion with '*'.

To detect the level of odd-order distortion, some of the odd excitation tones are set to zero. Odd-order nonlinear behavior turns odd frequency components in odd frequency components. This approach of using multisines to distinguish even- and odd-order nonlinear behavior is illustrated in Fig. 1.

To select the non-excited odd-frequency tones, the following strategy is followed: the odd frequencies are split into groups of three consecutive odd harmonics. Per group one randomly chosen component is set to zero. Proceeding in this way, the stochastic contribution at the non-excited frequencies is equal to the stochastic contribution at the excited frequencies [3].

B. Best linear approximation

The proposed methodology also allows to determine the propagation of distortion by each circuit element. Linear systems satisfy

$$B(f) = X_0(f) \cdot A(f) \tag{2}$$

where $A(f)$ and $B(f)$ represent the input and output, while $X_0(f)$ represents the transfer function of the linear system. For nonlinear systems (Fig. 1), it is no longer possible to satisfy this linear relationship. However, it is possible to approximate $X_0(f)$ by the best linear approximation (BLA) in the least square sense if a circuit remains mainly linear. For most Single Input Single Output (SISO) systems, excited with the random multisine with N in Eq. 1 sufficiently large, a transfer function can be obtained [2] of the form:

$$X(f_k) = X_0(f_k) + X_B(f_k) + X_S(f_k) \tag{3}$$

with

- X_0 the transfer function of the underlying linearized system (linearization around the quiescent operating point);
- X_B the systematic deviation between the linear behavior and the compression (or expension) of each sinusoid due to odd-order nonlinear behavior;
- X_S the stochastic nonlinear contribution, which has a zero mean if taken over different phase realizations of the excitation.

In other words, the expression $X_0 + X_B$ is the BLA.

C. Nonlinear subcircuit contribution

To calculate the distortion contribution of a subcircuit such as a transistor, inside a circuit, we excite the complete circuit with a multisine (Fig. 2). A transient analysis is applied, and over several (p) periods ($T_0 = 1/f_1$) we sample the waveforms of the input quantity $a_{in}(t)$ and the output quantity $b_{out}(t)$ of each nonlinear subcircuit. For each period i, these time-domain samples are transformed to the frequency domain, yielding the quantities $A_{in,i}(f)$ and $B_{out,i}(f)$, respectively. Finally, this data is averaged, yielding the frequency-domain quantities $\hat{A}_{in}(f)$ and $\hat{B}_{out}(f)$, respectively. For example, $\hat{A}_{in}(f)$ is given by

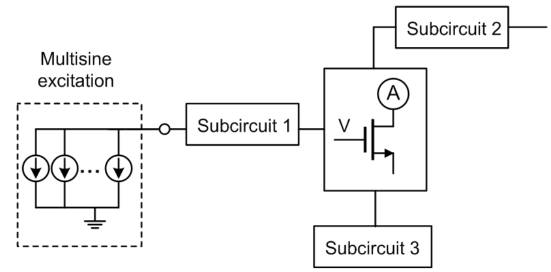

Fig. 2. A general analysis setup to determine the distortion contribution of a circuit element to its output nonlinearity.

$$\hat{A}_{in}(f) = \frac{1}{p} \cdot \sum_i A_{in,i}(f) \tag{4}$$

For $\hat{B}_{out}(f)$ a similar expression can be written. The best linear approximation $G(f_{EXC})$ for the input-output relationship of the subcircuit is calculated from

$$G(f_{EXC}) \cdot \hat{A}_{in}(f_{EXC}) = \hat{B}_{out}(f_{EXC}) \tag{5}$$

with f_{EXC} being the excited (odd) frequencies. To compare the contributions from the different subcircuits, the output quantity of each subcircuit is multiplied with the BLA from this output to the overall circuit output.

For a common-source and common-drain MOS transistor, the input quantity is a voltage, whereas the output quantity is a current. For a common-gate transistor, both input and output quantities are currents. Note that we consider the transistors as SISO transadmittance devices, not as MIMO subsystems. Although a full MIMO analysis [4] is more precise at the expense of complexity and simulation time, SISO analysis is sufficient for our purposes here.

D. Spectrum correction

If G would be excited by the selected odd-order tones only, we would find the distortion contributions on the designated frequencies. However, input power is available on non-excited frequencies due to nonlinear contribution of previous subcircuits. A first-order correction is applied by removing their linear contribution from the spectrum $\hat{B}$ as:

$$B_{corr}(f_{NEXC}) = \hat{B}(f_{NEXC}) - G(f_{NEXC}) \cdot \hat{A}_{in}(f_{NEXC}) \tag{6}$$

with f_{NEXC} the non-excited frequencies. Here, $G(f_{NEXC})$ is found by interpolation of $G(f_{EXC})$. Indeed, the linear contribution of non-excited tones present at the input are removed.

The difference between $B(f_{EXC})$ and $B_{corr}(f_{NEXC})$ is the distortion contributed by the subcircuit under observation.

E. Conclusion

We now have a means to distinguish odd- and even-order nonlinear behavior and the contribution of every nonlinear component in a circuit. The complexity is limited to a transient simulation. The analysis is valid for both weakly and strongly nonlinear distortion effects and wideband (practical) excitation signals.

III. Selective Volterra analysis

For Volterra series analysis, every nonlinearity is described as a power series. For example, the power series expansion of the drain current i_{ds} of a MOS transistor, which, in general, is a function of three voltages, v_{gs}, v_{ds} and v_{sb}, is given by

$$\begin{aligned} i_{ds} = \; & g_m \cdot v_{gs} + K_{2_{g_m}} \cdot v_{gs}^2 + K_{3_{g_m}} \cdot v_{gs}^3 + g_{ds} \cdot v_{ds} \\ & + K_{2_{g_{ds}}} \cdot v_{ds}^2 + K_{3_{g_{ds}}} \cdot v_{ds}^3 - g_{mb} \cdot v_{sb} - K_{2_{g_{mb}}} \cdot v_{sb}^2 \\ & - K_{3_{g_{mb}}} \cdot v_{sb}^3 + K_{2_{g_m \& g_{mb}}} \cdot v_{gs} \cdot v_{sb} \\ & + K_{3_{2g_m \& g_{mb}}} \cdot v_{gs}^2 \cdot v_{sb} + K_{3_{g_m \& 2g_{mb}}} \cdot v_{gs} \cdot v_{sb}^2 \\ & + K_{2_{g_m \& g_{ds}}} \cdot v_{gs} \cdot v_{ds} + K_{3_{2g_m \& g_{ds}}} \cdot v_{gs}^2 \cdot v_{ds} \\ & + K_{3_{g_m \& 2g_{ds}}} \cdot v_{gs} \cdot v_{ds}^2 + K_{2_{g_{mb} \& g_{ds}}} \cdot v_{sb} \cdot v_{ds} \\ & + K_{3_{2g_{mb} \& g_{ds}}} \cdot v_{sb}^2 \cdot v_{ds} + K_{3_{g_{mb} \& 2g_{ds}}} \cdot v_{sb} \cdot v_{ds}^2 \\ & + K_{3_{g_m \& g_{mb} \& g_{ds}}} \cdot v_{gs} \cdot v_{sb} \cdot v_{ds} + \ldots \end{aligned} \tag{7}$$

The coefficients K_2 and K_3 in this series are referred to as second- and third-order nonlinearity coefficients. They are proportional to second- and third-order derivatives, respectively, of the drain current with respect to one or more voltages. For example

$$K_{2_{g_m}} = \frac{1}{2} \cdot \frac{\partial^2 i_{DS}}{\partial v_{GS}^2} \quad \text{and} \quad K_{3_{g_m}} = \frac{1}{6} \cdot \frac{\partial^3 i_{DS}}{\partial v_{GS}^3} \tag{8}$$

According to Volterra theory [8], nonlinear behavior of a given order n can be expressed in terms of the multidimensional Fourier transform of the Volterra kernel of order n, which is a function of n frequency variables. These kernel transforms are found by summing the contribution from each nonlinearity coefficients of order 2 to n. Such contribution depends on the nonlinearity coefficient, on the lower-order response of the voltage that controls the nonlinearity and on the linear transfer function from the nonlinearity to the output of interest. Although a Volterra approach has proven to yield insight into weakly nonlinear circuit behavior [5], it suffers from a high complexity, due to the large number of contributions in practical CMOS circuits. Indeed, for a transistor not only the drain current depends on three voltages, but also the intrinsic capacitances are threedimensional nonlinearities. For order $n = 3$, each threedimensional nonlinearity gives rise to sixteen contributions.

In [5], all contributions are computed, and insight is obtained by sorting the contributions in descending order according to their magnitude and plotting the largest ones as a function of frequency. In this work, however, we compute an approximate value of the Volterra kernel transforms of each order by only taking into account the contributions from the main nonlinear components identified by the multisine analysis. The error on the approximation is verified by computing the nonlinear response (e.g. third-order intermodulation product, IIP_3) in terms of Volterra kernels [8] with the approximate kernels and comparing these responses with a two-tone simulation in SpectreRF® [7] at small input amplitude to ensure weakly nonlinear behavior.

The nonlinearity coefficients (Eq. 7 and 8) are computed by numerical differentiation of DC parameters (currents and capacitors) from a DC simulation with Spectre of one transistor over a range of values of v_{GS}, v_{DS} and v_{DS}.

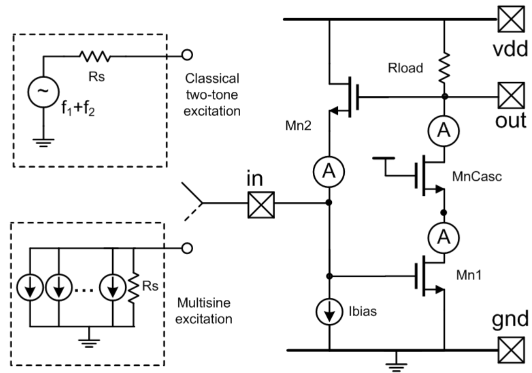

Fig. 3. Simplified schematic of the 90 nm LNA with classical two-tone and proposed multisine excitation signals.

IV. Design example

To illustrate the proposed methodology, we designed a 90 nm low-noise amplifier (Fig. 3). Since the supply voltage lowers drastically when scaling CMOS, this circuit is vulnerable to nonlinear behavior. Indeed, transistors are pushed into lower degrees of inversion, causing higher levels of weakly nonlinear distortion. Furthermore, clipping, which is strongly nonlinear behavior, occurs faster.

A. Two-tone analysis

As a classical way of determining the distortion in the circuit, a two-tone test is performed in SpectreRF using MOS Model 11 [1] models of the 90 nm transistors. The (arbitrarily) selected excitation tones are 1 GHz and 1.2 GHz. The *IIP3* is -13 dBm (see Fig. 4), possibly unsatisfactory, since wideband amplifiers generally require high linearity specs. Trying to improve the linearity is difficult when the designer lacks insight in the distortion mechanisms in the particular circuit and their propagation through the circuit. Insight is complicated by the nonlinear feedback via Mn2 and the large number of nonlinearity sources. Whether this feedback is helping or worsening the linearity is not obvious [8].

B. Multisine analysis

The circuit is excited by a multisine source, as illustrated in Fig. 3. The excited frequency band is chosen from 100 MHz

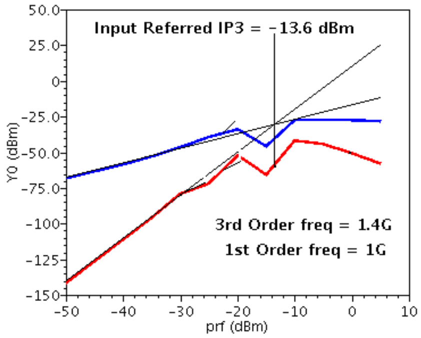

Fig. 4. Two-tone analysis on the amplifier.

to 7 GHz, with a tone separation of 25 MHz. We thus have a multisine of 92 tones for which a uniform amplitude is chosen. A transient analysis is performed in SpectreRF using the same transistor models as before. This analysis, from which all data is extracted, requires 279 seconds on a HPUX9000 platform. The node voltages, as well as the currents indicated on Fig. 3 with Ⓐ are sampled. For every period of the sampled signals (after the transients have died out), an FFT is calculated. The resulting spectra are averaged.

Fig. 5(a) plots the spectrum of the input and output nodes, averaged over the selected periods. The best linear approximation is indicated by '·'. Nonlinear contributions are indicated with '+' and 'o'. Note that the clouds of '+' and 'o' would converge to a line if the amplitudes are averaged over sufficient experiments with different phase realizations of the multisine.

One can observe a vast amount of distortion present in the output spectrum. In fact, the even-order distortion (+) is only 10 dB lower than the response at the excited frequency tones (·) and the odd-order distortion (o) is 20 dB lower. Also noticeable is a large amount of nonlinear components in the input spectrum. With only this information — comparable to classical distortion simulation — it is still challenging to track the major source of nonlinearity.

To gain insight in the distortion propagation, we calculate the contribution of all transistors to the output distortion. Similar to Eq. 5, the BLA of transistor Mn1 is calculated as:

$$G_{Mn1}(f_{EXC}) = \frac{\hat{I}_{d,Mn1}(f_{EXC})}{\hat{V}_{in}(f_{EXC})} \tag{9}$$

with $\hat{I}_{d,Mn1}$ the FFT of the current sampled at the drain of Mn1, and $\hat{V}_{in}$ the FFT of the voltage sampled at the gate of Mn1 (both averaged over some periods of the multisine). We find (similar to Eq. 6):

$$\begin{aligned} &I_{d,Mn1,corr}(f_{NEXC}) = \\ &\hat{I}_{d,Mn1}(f_{NEXC}) - G_{Mn1}(f_{NEXC}) \cdot \hat{V}_{in}(f_{NEXC}) \end{aligned} \tag{10}$$

Here, $G_{Mn1}(f_{NEXC})$ is found by linear interpolation of $G_{Mn1}(f_{EXC})$. To find the contribution to the circuit's output, we multiply with the BLA from this current to the output

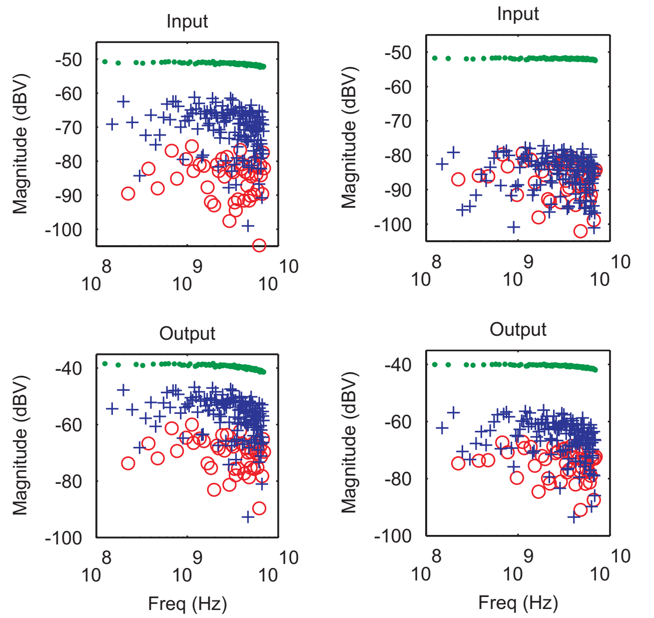

(a) Before (b) After

Fig. 5. Input and output spectrum of the transient analysis, before and after linearity optimization. Excited tones are marked with '·', even-order distortion with '+' and odd-order distortion with 'o'.

voltage of the circuit. This BLA is given by:

$$G_{Mn1.Out}(f_{EXC}) = \frac{\hat{V}_{out}(f_{EXC})}{\hat{I}_{d,Mn1}(f_{EXC})} \tag{11}$$

We find:

$$\begin{aligned} \hat{V}_{contr.Mn1}(f_{EXC}) &= \hat{I}_{d,Mn1}(f_{EXC}) \cdot G_{Mn1.Out}(f_{EXC}) \\ &= \hat{V}_{out}(f_{EXC}) \end{aligned} \tag{12}$$

which is nothing else than the output spectrum. The distortion contributions from Mn1 are given by:

$$\begin{aligned} &\hat{V}_{contr.Mn1}(f_{NEXC}) = \\ &\hat{I}_{d,Mn1,corr}(f_{NEXC}) \cdot G_{Mn1.Out}(f_{NEXC}) \end{aligned} \tag{13}$$

The contributions of all transistors are plotted in Fig. 6(a). From this figure, we derive that Mn2 is the major contributor to the overall nonlinear behavior. It is also seen that Mn2 produces much even-order distortion, which is fed back to the circuit input. This distortion is in turn converted into (even- and odd-order) distortion at the output. To increase the linearity of the circuit, we thus have to decrease the contribution of Mn2.

The large contribution of Mn2 can be understood since the signal swing at the output (which is the "input" of Mn2) is larger than at the input. Clipping at the input of Mn2 would be translated into a strong contribution of MnCasc. Clipping at the output of Mn2 is then again unlikely, since only minor signal swing is present at the circuit's input. Since MnCasc generates little distortion, Mn2's distortion is mainly due to the excited frequency components. This distortion is thus most probably due to the second-order nonlinearity of Mn2. Therefore, by

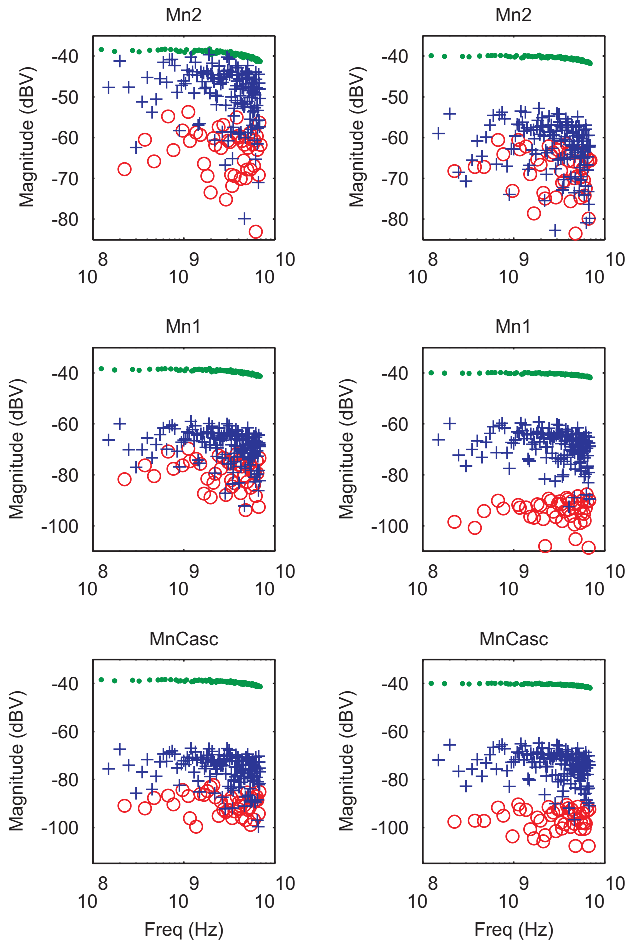

(a) Before (b) After

Fig. 6. Each transistor's best linear approximation and nonlinearity contribution to the circuit's output, before and after linearity optimization. Excited tones are marked with '·', even distortion with '+' and odd distortion with 'o'.

increasing Mn2's overdrive, we expect to substantially improve the circuit's linearity.

Adapting the design of the circuit, we increase the overdrive of Mn2 by 250 mV. As Fig. 5(b) shows, the output distortion is now substantially reduced, both the even- and the odd-order ones. Looking at the contribution of Mn2 in Fig. 6(b), it is clear that Mn2 now generates much less distortion, meaning that we successfully located the cause of nonlinearity.

The careful reader might also notice that odd-order distortion of Mn1 has been lowered in the redesign. This is perhaps surprising, since no effort has been made to lower Mn1's nonlinearity. The effect can be atributed to the even-order nonlinearity in Mn2. Indeed, before the redesign, even-order contributions of Mn2 were almost as large as the linear contributions (odd). These two (odd and even) cause odd-order distortion generated by Mn1. Yet these distortions are not compensated by Eq. 6. As a consequence, when even-order nonlinearity of Mn2 lowers, less odd-order distortion is generated by Mn1.

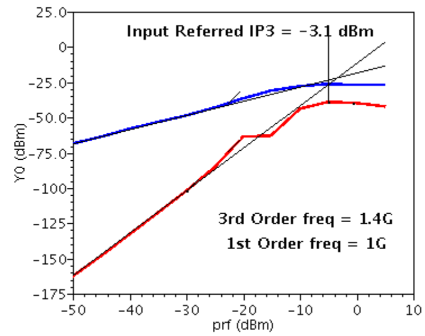

Fig. 7. Two tone analysis on the amplifier, after the linearity optimization.

To validate the redesign and the multisine methodology, the two-tone test is repeated for the optimized circuit, as presented in Fig. 7. The IIP3 is now -3.1 dBm, which is about 10 dB better than the initial circuit. This indicates that we took the appropriate design action to lower the distortion.

To further clarify insight in nonlinear operation, a selective Volterra analysis can be used, as explained in the next section.

C. Selective Volterra analysis

In this section, we first discuss the result of a full Volterra analysis of the LNA without omitting any contribution, in order to check the conclusions from the multisine analysis in Section IV-B. We compute second- and third-order kernel transforms in the LNA. The same two-tone analysis has been carried out as in Fig. 4. The IIP_3 is computed from the third-order Volterra kernel of the output voltage, $H_3(j\omega_1, j\omega_1, -j\omega_2)$ with $\omega_1 = 2\pi \cdot 1.2\,GHz$ and $j\omega_2 = 2\pi \cdot 1\,GHz$. Table I compares the results, which match very well to the SpectreRF simulations. From a plot of the main contributions (Fig. 8) to the third-order intermodulation product at $1.4\,GHz$, we find that the second-order nonlinearity coefficient $K_{2_{g_m}}$ of Mn2 yields the largest contribution. This contribution is proportional to the second-order kernel of $v_{GS\,Mn2}$, which is the controlling voltage of the nonlinearity on g_{mMn2}. The second-order nonlinearity $K_{2_{g_m}}$ of Mn2 combines this second-order kernel of $v_{GS\,Mn2}$ with the first-order signal of $v_{GS\,Mn2}$ to produce a third-order signal. Analysis of the second-order kernel of $v_{GS\,Mn2}$ points out that this kernel is also mainly determined by $K_{2_{g_m\,Mn2}}$. This corresponds to the observations from Section IV-B. Next, the approximate Volterra kernels are computed, using only the contributions of the sixteen nonlinearity coefficients of the drain current of Mn2. This computation is performed in Matlab in 2.9 seconds. The deviation on the IIP_3 (Table I) between the exact analysis and the approximate one is 0.9 dB.

Using the two main contributions of Mn2 ($K_{2_{g_{mMn2}}}$ and $K_{3_{g_{mMn2}}}$), an approximate expression for IIP_3 can be derived with symbolic network analysis. One finds for IIP_3 expressed

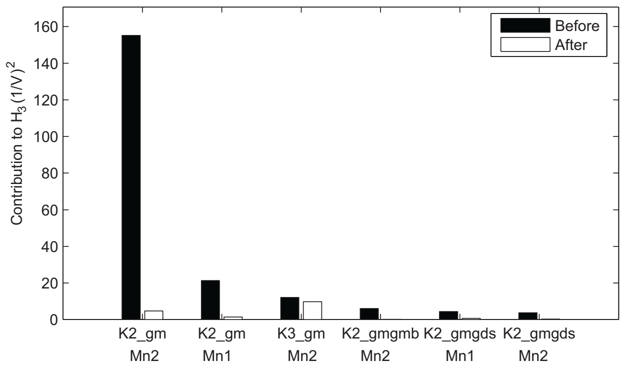

Fig. 8. Dominant nonlinearity contributors to the third-order Volterra Kernel $|H_3(j\omega_1, j\omega_1, -j\omega_2)|$.

	SpectreRF	Full Volterra	Selective Volterra	Eq. (14)
Before	-13.6	-13.5	-12.6	-14.4
After	-3.1	-3.1	-2.7	-0.7

TABLE I

IIP3 CALCULATION OVERVIEW IN dBm

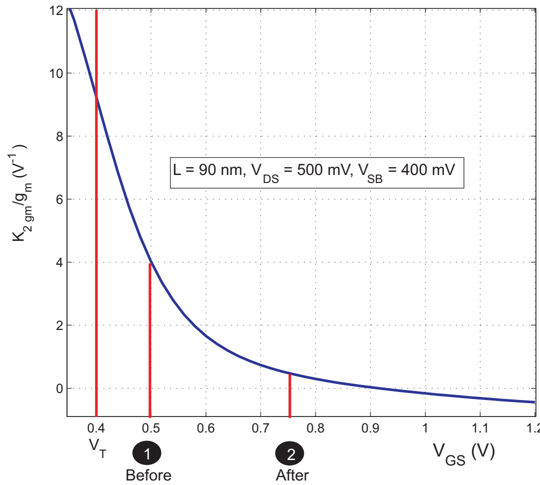

Fig. 9. Normalized second-order nonlinearity coefficient $K_{2_{g_m}}/g_m$ as a function of the inversion level. Point 1 and 2 correspond to the original operating point of Mn2 in the LNA, and the point with the higher IIP_3, respectively.

in terms of the amplitude of the input voltage source:

$$IIP_3 = \frac{4}{1+A_V} \cdot \sqrt{\frac{2}{3\left[\left(\frac{K_{2_{gmMn2}}}{g_{mMn2}}\right)^2 + \frac{K_{3_{gmMn2}}}{g_{mMn2}}\right]}} \quad (14)$$

in which

$$A_V = g_{m\,Mn1} \cdot R_{load} \quad (15)$$

is the circuit voltage gain. This formula tells us that IIP_3 can be increased by decreasing the gain or by decreasing the second- and third-order nonlinearity coefficients of Mn2, normalized to g_{mMn2}. In the original design point, the term with $(K_{2_{gmMn2}}/g_{mMn2})^2$ in the denominator dominates. From Fig. 9 we see that by shifting the original bias point from $V_{GS} = 0.5\,V$ (moderate inversion) to $V_{GS} = 0.75\,V$ (strong inversion), the normalized second-order coefficient $K_{2_{gmMn2}}/g_{mMn2}$ is much lower. In this way, the second-order Volterra kernel of $v_{GS\,Mn2}$ is also lower, yielding in turn a reduction of $H_3(j\omega_1, j\omega_1, -j\omega_2)$. A look at the dominant contributions to the latter kernel in this new design point (see Fig. 8) shows that the contribution of $K_{2_{gmMn2}}$ has been reduced, even below the contribution of $K_{3_{gmMn2}}$.

Table I list the evaluation of Eq. 14. Before the redesign this formula is fairly accurate. The inaccuracy on the formula after redesign is due to the lower relative contribution of $K_{2_{gmMn2}}$ (see Fig. 8).

This example illustrates how selective Volterra analysis yields added detailed insight in weakly nonlinear circuit behavior to the multisine analysis. The latter can be regarded as a powerful preprocessor to greatly simplify Volterra analysis.

V. CONCLUSIONS

To gain insight into nonlinear circuit behavior, this work demonstrates an approach that can split this behavior into different contributions, one for each nonlinear component such as a transistor. This approach, which uses multisine analysis, works both for weakly and strongly nonlinear behavior. For weakly nonlinear behavior, this approach is combined with Volterra series analysis: using the selection of the main nonlinear components with the multisine analysis, the complexity of the Volterra analysis is seriously reduced, as it only needs to compute the contributions of few nonlinearities to the observed nonlinear response. The design example reported here, namely a 90 nm CMOS wideband LNA, shows that the combined approach yields clear guidelines to reduce nonlinear distortion of a practical circuit.

ACKNOWLEDGMENT

This work was supported by the Institute for the Promotion of Innovation through Science and Technology in Flanders (IWT Vlaanderen). This research was funded by a grant of the Fund for Scientific Research (FWO-Vlaanderen), the Flemish Government (GOA-IMMI), the Belgian Program on Interuniversity Poles of attraction initiated by the Belgian State, Prime Minister's Office, Science Policy programming (IUAP V/2) and the research council of the VUB (OZR). The research reported in this paper was performed in the context of the Top Amplifier Research Groups within a European Team (TARGET) network.

REFERENCES

[1] Mos Model 11. *http://www.semiconductors.philips.com/Philips_Models/mos_models/model11.*

[2] J. Schoukens et al. Linear modeling in the presence of nonlinear distortions. *IEEE Trans. Instrum. Meas.*, 16(4):786–792, August 2002.

[3] K. Vanhoenacker et al. Design of multisine excitations to characterize the nonlinear distortions during frf-measurements. *IEEE Trans. Instrum. Meas.*, 50(5):1097–1102, October 2001.

[4] L. De Locht et al. Identifying the main nonlinear contributions: use of multisine excitations during circuit design. *ARFTG Microwave Measurements Conference*, pages 75–84, December 2004.

[5] P. Dobrovolný et al. Analysis and compact behavioral modeling of nonlinear distortion in analog communication circuits. *IEEE Trans. Computer-Aided Design 22(9)*, 22(9):1215–1227, September 2003.

[6] P. Li and L. Pileggi. Efficient per-nonlinearity distortion analysis fior analog and rf circuits. *IEEE Trans. Computer-Aided Design 22(9)*, 22(10):1297–1309, October 2003.

[7] SpectreRF. *http://www.cadence.com/products/custom_ic/spectrerf.*

[8] P. Wambacq and W. Sansen. *Distortion Analysis of Analog Integrated Circuits, 1st ed.* Kluwer Academic Publishers, Harlow, England, 1998.